Cirrus induced polarization in 122 GHz aura Microwave Limb Sounder radiances

C. P. Davis,[1] D. L. Wu,[2] C. Emde,[3] J. H. Jiang,[2] R. E. Cofield,[2] and R. S. Harwood[1]

Received 16 February 2005; revised 28 May 2005; accepted 20 June 2005; published 20 July 2005.

[1] Previous simulation studies have outlined the possibility of significant polarization signals in microwave limb sounding due to horizontally aligned ice crystals in cirrus clouds. From the recently launched Aura MLS instrument, we present the first polarized microwave limb sounding observations of cirrus clouds. We also present polarized radiative transfer simulations, which show qualitative agreement with these observations, and indicate the limits to which aligned non-spherical particles are influencing bulk optical properties of cirrus clouds at microwave wavelengths. Although 122 GHz is not ideal for cloud measurements due to strong O_2 absorption, data and simulations suggest that preferential crystal orientation is causing small, but noticeable, partial vertical polarization, which can be replicated in simulations by considering all particles as horizontally aligned oblate spheroids with aspect ratios of around 1.2 ± 0.15. **Citation:** Davis, C. P., D. L. Wu, C. Emde, J. H. Jiang, R. E. Cofield, and R. S. Harwood (2005), Cirrus induced polarization in 122 GHz aura Microwave Limb Sounder radiances, *Geophys. Res. Lett.*, *32*, L14806, doi:10.1029/2005GL022681.

1. Introduction

[2] The EOS Aura Microwave Limb Sounder (MLS) has been fully operational since 13 August 2004. Aura MLS makes daily global measurements of stratospheric temperature, geopotential height, water vapour, O_3, OH, HO_2, CO, HCN, CH_3CN, N_2O, HNO_3, HCl, HOCl, ClO, BrO, and volcanic SO_2. Several of these measurements are also made in the mid- to upper-troposphere [e.g., *Waters et al.*, 1999]. Ice clouds can adversely affect these tropospheric measurements. On the other hand, the effect of cirrus on received radiances can provide information on cloud properties; indeed, ice water content (IWC) has been included as a MLS data product.

[3] A thorough treatment of the effect of cirrus on MLS measurements requires the consideration of polarization. *Czekala* [1998] showed that of all possible viewing geometries, limb sounding would be most affected by cloud induced polarization where there are non-spherical preferentially aligned ice crystals. *Miao et al.* [2003] studied the utilization of cirrus induced polarization in a possible slant viewing mm/sub-mm cloud sensor. To investigate the polarization effect on Aura MLS, a 3D polarized forward model was developed [*Davis et al.*, 2005] and incorporated into the ARTS software package (http://www.sat.uni-bremen.de/arts).

[4] *Czekala* [1998], *Miao et al.* [2003], *Davis et al.* [2005], and *Emde et al.* [2004], have all shown that the orientation distribution is the dominant factor in determining the magnitude of the polarization signal. However, the extent to which preferentially aligned non-spherical particles affect the bulk optical properties of cirrus clouds at microwave frequencies is unknown. It is well known that falling plate and column crystals have a preferred horizontal orientation, but in cirrus clouds pristine crystals (plates, columns) are generally outnumbered by aggregates [e.g., *Baran*, 2004], which have an infinite variety of complex shapes, and whose orientation behaviour is unclear. The presence of large randomly oriented particles will strongly dilute the polarizing influence of horizontally aligned pristine crystals. Using a ice crystal aggregation model [*Westbrook et al.*, 2004] showed that as aggregates grew, they asymptotically approached an aspect ratio of 0.65 ± 0.05, which agreed well with in situ observations. It seems reasonable to postulate that such aggregate particles may have a preferred orientation with the longest dimension parallel to the horizontal, but that the orientation distribution will be broader than that of pristine particles. Measurements of solar reflectance by the POLDER/ADEOS instrument [*Chepfer et al.*, 1999] indicated that horizontal ice crystal alignment was noticeable in 40% of cirrus observations.

[5] Space-borne off-nadir polarized mm/sub-mm observations of cirrus will help establish whether preferentially oriented ice crystals substantially affect the bulk optical properties of cirrus clouds. In turn, this information may impact on any future plans for any polarization based cirrus measurements [e.g., *Miao et al.*, 2003], and will help evaluate whether the computational expense of polarized radiative transfer is justified in retrieval software for space-borne off-nadir microwave instruments. In this paper we present the first such observations.

[6] The EOS-MLS instrument is on board the Aura spacecraft, which was successfully launched on 15 July 2004. The MLS instrument incorporates five radiometers with broad bands centred at 118 GHz, 190 GHz, 240 GHz, 640 GHz, and 2.5 THz, labelled R1 to R5 respectively. For cloud detection it is preferable to use window channels, where atmospheric absorption and emission is relatively weak. This gives cloud affected radiances the greatest contrast with those for clear-sky cases. In the case of low tangent heights, where the received radiation emanates from the lower troposphere in clear cases, clouds produce a significant brightness temperature depression due to scat-

[1]Institute of Atmospheric and Environmental Science, University of Edinburgh, Edinburgh, UK.
[2]Jet Propulsion Laboratory, California Institute of Technology, Pasadena, California, USA.
[3]Institute for Envronmental Physics, University of Bremen, Bremen, Germany.

0094-8276/05/2005GL022681$05.00

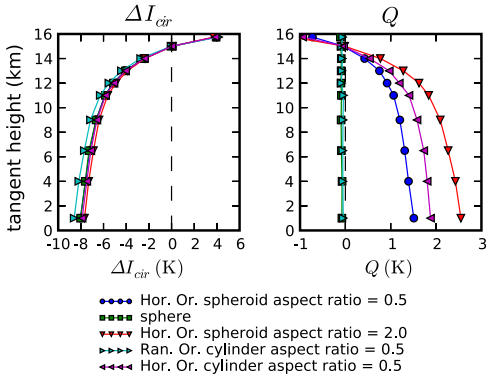

Figure 1. Example 122 GHz radiative transfer simulations for the 3D deep cirrus scenario with different shape/orientation combinations. In each case, the cloud has a uniform IWC of 0.2 gm^{-3}.

tering, and for high tangent heights, where the background is cold in clear sky cases, we can get a significant brightness temperature enhancement. Example window frequencies for Aura MLS are 200.5 GHz in R2, and 230 GHz in R3. However, in this study we use radiances from R1, because for this frequency range we are able to obtain both horizontally and vertically polarized components of the limb radiation. R1A and R1B have orthogonal antenna polarizations, V and H respectively, which relate to the electric field vector. The V axis corresponds to the direction that is perpendicular to the line of sight and lying on the plane containing the line of sight and the local zenith. For this study we choose data from channel 1 of band 32 (R1A), and band 34(R1B), which are single 0.5 GHz wide filters centred at 122 GHz. This channel is the furthest from the 118 GHz O_2 line, and therefore the most sensitive to cloud. Although this channel is not as sensitive to cirrus as some of those in R2 and R3, due to O_2 absorption and a relatively large wavelength to particle size ratio, high thick cirrus can cause brightness temperature depressions as large as 50 K for low tangent heights.

[7] In this paper, these channels are used to calculate the total radiance, $I = I_v + I_h$, and the polarization difference, $Q = I_v - I_h$, which characterises the degree of horizontal or vertical polarization. Polarized radiative transfer simulations using the ARTS software package are presented to help interpret the observed polarization data.

2. Polarized MLS RT Simulations for 122 GHz

[8] The intensity and polarization state of a beam of incoherent electromagnetic radiation is described by the Stokes' vector $\mathbf{I} = [I, Q, U, V]^T$. Here we express these parameters as Rayleigh Jeans brightness temperatures. Simulation of the Stokes vector for a given propagation direction $\mathbf{n}$ at the MLS antenna is achieved by solving the vector radiative transfer equation (VRTE) [e.g., *Mishchenko et al.*, 2000]:

$$\frac{d\mathbf{I}(\mathbf{n})}{ds} = -\mathbf{K}(\mathbf{n})\mathbf{I}(\mathbf{n}) + \mathbf{K_a}(\mathbf{n})I_b(T) + \int_{4\pi} \mathbf{Z}(\mathbf{n},\mathbf{n}')\mathbf{I}(\mathbf{n}')d\mathbf{n}' \quad (1)$$

s is distance along direction $\mathbf{n}$ and I_b is the Planck radiance. $\mathbf{K}(\mathbf{n})$, $\mathbf{K_a}(\mathbf{n})$, and $\mathbf{Z}(\mathbf{n}, \mathbf{n}')$ are the bulk extinction matrix, absorption coefficient vector and phase matrix of the medium respectively.

[9] In this study two algorithms are used for the solution of the VRTE. ARTS-DOIT [*Emde et al.*, 2004] is an iterative discrete ordinates type radiative transfer model, which calculates the Stokes vector for an array of directions at every grid point in the scattering domain. ARTS-MC, which employs a reversed Monte Carlo RT algorithm [*Davis et al.*, 2005], calculates the Stokes vector only for the desired sensor position and viewing direction. For 3D simulations ARTS-MC is generally preferred for its reduced CPU and memory requirements. For 1D simulations, which are generally much less demanding than 3D simulations, ARTS-DOIT is used. Crucial to the suitability of the ARTS platform for limb sounding simulations is its incorporation of 1D or 3D spherical geometry.

[10] In the following simulations two cloud types are considered: a 1D layer cirrus scenario with a cloud base at 11.9 km and a cloud top at 13.4 km; and a 3D deep cirrus scenario with a base at 6 km, a top at 16 km, and a horizontal extent of 50 km in zonal and meridional directions. For the sake of defining lines of sight (LOS), the 3D scenario is centered at (0N, 0E). The purpose of using these two different yet representative cloud scenarios, was to assess the generality of any interpretation of MLS polarization signals in terms of ice crystal shape and orientation. A single representative tropical profile is used for temperature and water vapour fields. Particle size distributions are obtained from ice water content (IWC) and temperature fields using the *McFarquhar and Heymsfield* [1997] size distribution for tropical cirrus. Single scattering properties for horizontally aligned non-spherical particles (spheroids or cylinders) are calculated using the PyARTS python package (http://www.met.ed.ac.uk/cory/PyARTS), which combines the *T*-matrix code of *Mishchenko* [2000], and the ice refractive index data of *Warren* [1984], to give $\mathbf{K}(\mathbf{n})$, $\mathbf{K_a}(\mathbf{n})$, and $\mathbf{Z}(\mathbf{n}, \mathbf{n}')$ in an ARTS readable format.

[11] The expected polarization behaviour of cirrus affected 122 GHz MLS radiances is demonstrated in Figure 1, which shows example 122 GHz radiative transfer simulations for the 3D deep cirrus scenario described above. Five different particle shape/orientation combinations were used: horizontally aligned prolate spheroids with aspect ratio 0.5, spheres, horizontally aligned oblate spheroids with aspect ratio 2.0, randomly aligned prolate cylinders with aspect ratio 0.5, and horizontally aligned prolate spheroids with aspect ratio 0.5. For the prolate particles, their axis of rotation is orientated randomly with respect to the azimuth. In each case, the cloud had a uniform IWC of 0.2 gm^{-3}. In these simulations the field of view characteristics of the Aura MLS antenna have not been explicitly considered; they consider only a pencil-beam. For the deep cirrus scenario, all lines of sight pass through a point near the top-center of the cloud (0N, 0E, 15.75 km), with tangent points in the cloud for high tangent points, and moving further behind the cloud (as viewed by the sensor) for low tangent heights. At (0N, 0E, 15.75 km) the LOS has a zenith angle of 90° for the 15.75 km tangent height, and a zenith angle of 93.89° for the 1 km tangent height.

[12] The first panel in Figure 1 indicates that the choice of particle type and orientation scheme has only a small relative effect on the cloud induced radiance, $\Delta I_{cir} = I_{cloudy} - I_{clear}$.

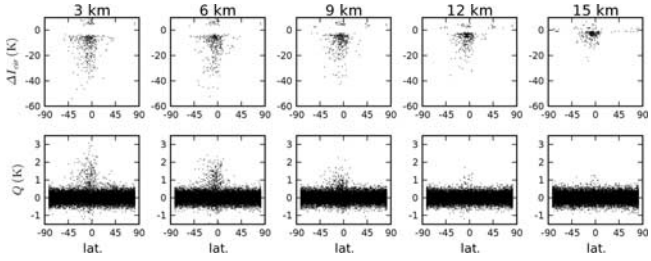

Figure 2. Cloud induced radiance, ΔI_{cir}, and polarization difference, Q, for January 3–8, 2005.

However, particle type, and orientation does have a significant impact on the polarization difference. Although randomly oriented prolate cylinders behave almost exactly like spherical particles (of the same volume), the horizontally aligned non-spherical particles give significant partial vertical polarization for low tangent heights.

[13] The sign of the polarization signal is determined by the magnitude of two mechanisms: dichroism, which is the effect of a non-diagonal extinction matrix, **K**; and the effect of radiation being scattered into the line of sight, which is described by the last term in equation (1). For the scenarios shown in Figure 1 the cloud optical depth, $\tau = K_{11}s$, increases from around 0.28 at 1 km tangent height to 0.42 at 15.75 km. So in this case the simulation results can be well understood using the small τ approximation for the Q value exiting the cloud,

$$Q \approx \left(J_Q - K_{12}I_0\right)s, \tag{2}$$

where

$$J_Q = K_{a2}(\mathbf{n})I_b(T) + \int_{4\pi} Z_{2i}(\mathbf{n},\mathbf{n}')I_i(\mathbf{n}')d\mathbf{n}', \tag{3}$$

which is evaluated at a particular point on the line of sight within the cloud. In the derivation of equation (2), **K** is assumed to be constant along the propagation path. J_Q depends on the shape and orientation of the scattering particles, as well as the angular distribution of incoming radiation. For these simulations, J_Q is negative, and relatively independent of the tangent height since all lines of sight pass through the same region of the cloud, with very similar propagation directions. However, the radiance entering the cloud, I_0, varies considerably with tangent height; from 235 K at 1 km, to 90 K at 15.75 km. So for horizontally aligned particles, where K_{12} is negative, we get positive Q for low tangent heights due to the large values of I_0 and the resulting dominance of second term in equation (2). For spherical and randomly oriented particles, **K** is diagonal, so Q is solely determined by J_Q.

[14] A small τ approximation can also be easily derived for ΔI_{cir}:

$$\Delta I_{cir} \approx \left(J_I^c - K_{11}^c I_0\right)s, \tag{4}$$

where $J_I^c = J_I - k_g I_b(T)$, J_I is analogous to J_Q (equation (3)) but for the 1st Stokes component, k_g is the gaseous absorption coefficient, and $K_{11}^c = K_{11} - k_g$. Hence, the c superscript signifies the portion of J_I and K_{11} due to the presence of cloud particles. Equations (2) and (4) suggest that low tangent height R1 observations of cirrus clouds can be adequately simulated by choosing a particle ensemble with the appropriate K_{11} and K_{12} values. This is easily achieved by using horizontally aligned oblate spheroids with an appropriate aspect ratio.

3. Example Aura MLS Observations of Q for 122 GHz

[15] ΔI_{cir} and Q can be obtained from Aura MLS level 1B (L1B) radiance files. A daily L1B file contains data for 14 orbits which is comprised of approximately 3495 limb scans, or major frames (MAFs), which in turn contain 125 minor frames (MIFs). For R1, the MLS field of view corresponds to a tangent height range of approximately 6.5 km. Some steps are needed to refine the R1A and R1B radiometric calibration for accurate Q calculation. Firstly, any bias in the R1A-R1B space-view radiances are removed by subtracting the mean of brightness temperatures for tangent heights greater than 50 km. Secondly we apply a 3.5% gain correction to the R1B radiances for MLS L1B versions 1.5 and older. After making these corrections to T_b^{R1A} and T_b^{R1B}, I and Q are given by $0.5(T_b^{\mathrm{R1A}} + T_b^{\mathrm{R1B}})$ and $0.5(T_b^{\mathrm{R1A}} - T_b^{\mathrm{R1B}})$ respectively. Finally, to calculate the cloud induced radiance, ΔI_{cir}, we pass I values for all the MAFs for each tangent height through a high pass filter. This separates radiance variation due to clouds from latitudinal clear sky radiance variation. Q is also high pass filtered to remove remaining second order effects related to the R1A/R1B gain mismatch. In both cases the high pass filter involves subtracting the result of a median filter, with a window 19 MAFS (approx. 3000 km), from the original data.

[16] In Figure 2 ΔI_{cir} and Q are shown for 3–8 January 2005. Figure 2 shows a high frequency of cloud affected radiances in a region centred slightly south of the equator. This can be be explained by the inability of R1 to detect low clouds, and the prevalence of high ice clouds due to the position of the inter-tropical convergence zone and the region of increased tropopause height, which are consistent with the northern hemisphere winter. Clear sky variance has been screened from the ΔI_{cir} in Figure 2 by only including points that differ from zero by more than 2σ. In the second row of Figure 2 we see a region with observations of partial vertical polarization (positive Q) coinciding with the latitude range of cloud induced ΔI_{cir}. The variation in ΔI_{cir} and Q with tangent height are in qualitative agreement with the example RT simulations shown in Figure 1; the observations exhibit negative ΔI_{cir} and small positive Q for low tangent heights, with the magnitude of both decreasing with increasing tangent height. As shown in section 2, this behaviour is well explained by the small τ approximations, equations (2) and (4). The period of January 3–8 was chosen for its relative lack of disturbances due to spacecraft operations and other anomalies. In every other respect the behaviour shown in Figure 2 is typical for all days to date, except for the meridional distribution of cloud events, which varies seasonally.

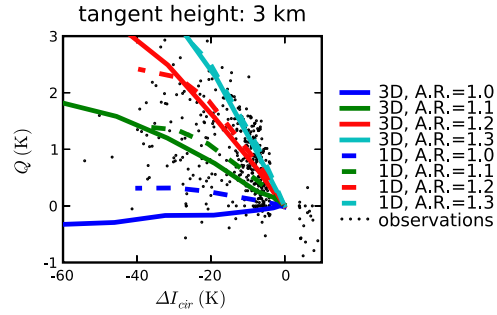

Figure 3. Observed and simulated Q vs. ΔI_{cir}. The axis limits reflect the range of observations, so a significant portion of some simulation curves are not shown.

[17] In Figure 3 the association of the partial vertical polarization with clouds is clarified by plotting Q against ΔI_{cir}. Only cloudy points, where $|\Delta I_{cir}| > 2\sigma$, are shown. We see that a majority of the cloudy points have positive Q values, indicating partial vertical polarization.

[18] Also shown in Figure 3 are simulated Q vs. ΔI_{cir} curves for horizontally aligned oblate spheroids with aspect ratios 1.0(spheres), 1.1, 1.2 and 1.3. Each curve represents a range of IWC from 0.01 gm^{-3}, which has negligible effect on the simulated Stokes vector, to 1 gm^{-3}. Curves are shown for both the 3D deep (solid) and 1D layer (dashed) cirrus scenarios described above. The curves for the two cloud shapes become more similar as the particles become more nonspherical. The 1D layer curves appear shorter due to the increased gaseous absorption between the cloud and the sensor.

[19] Most data points lie between the simulation curves for aspect ratios 1.1 and 1.3, which indicates that the bulk extinction matrix is noticeably non-diagonal, indicating an influence from oriented particles. The spread of the clear-sky Q values in Figure 2 indicates a low signal to noise ratio for the cloud induced polarization. However, from these results it seems reasonable to conclude that the Stokes vector for cloud affected 122 GHz MLS measurements can be adequately reproduced by considering all hydrometeors as horizontally aligned oblate spheroids with aspect ratio 1.2 ± 0.15. This interpretation is not dependent on the choice of simulated cloud scenarios.

4. Conclusion

[20] Because of strong gaseous absorption, 122 GHz is not particularly sensitive to clouds, yet these observations show a noticeable cirrus induced polarization. For window channels this signal will be larger. Q values become particularly interesting for window frequencies in R2 and R3, because these radiometers have orthogonal polarizations, V and H respectively.

[21] The results presented here for 122 GHz suggest the possibility of retrieving cirrus particle shape/orientation information. Cirrus crystal shape and orientation have a significant importance when considering the impact of cirrus on the earth's radiation budget [e.g., *Takano and Liou*, 1989]. The retrieval of cirrus particle shape and orientation information from Aura MLS data is a topic for further study.

[22] **Acknowledgments.** The authors wish to thank the entire Aura MLS team and the developers of the ARTS software package. Thanks are also due to Michael Mishchenko and Stephen Warren for the availability of the *T*-matrix and ice refractive index codes respectively. This paper was improved considerably thanks to comments by the anonymous reviewers. Cory Davis is funded by the Natural Environment Research Council (UK) under the Clouds Water Vapour and Climate thematic programme.

References

Baran, A. (2004), On the scatting and absorption properties of cirrus cloud, *J. Quant. Spectrosc. Radiat. Transfer*, *89*, 17–36.

Chepfer, H., G. Brogniez, P. Goloub, F. Breon, and P. Flamant (1999), Observations of horizontally oriented ice crystals in cirrus clouds with POLDER-1/ADEOS-1, *J. Quant. Spectrosc. Radiat. Transfer*, *63*, 521–543.

Czekala, H. (1998), Effects of ice particle shape and orientation on polarized microwave radiation for off nadir problems, *Geophys. Res. Lett.*, *25*, 1669–1672.

Davis, C., C. Emde, and R. Harwood (2005), A 3D polarized reversed Monte Carlo radiative transfer model for mm and sub-mm passive remote sensing in cloudy atmospheres, *IEEE Trans. Geosci. Remote Sens.*, *43*, 1096–1101.

Emde, C., S. A. Buehler, C. Davis, P. Eriksson, T. R. Sreerekha, and C. Teichmann (2004), A polarized discrete ordinate scattering model for simulations of limb and nadir long-wave measurements in 1-D/3-D spherical atmospheres, *J. Geophys. Res.*, *109*, D24207, doi:10.1029/2004JD005140.

McFarquhar, G., and A. Heymsfield (1997), Parametrization of tropical ice crystal size distributions and implications for radiative transfer: Results from CEPEX, *J. Atmos. Sci.*, *54*, 2187–2200.

Miao, J., K.-P. Johnson, S. Buehler, and A. Kokhanovsky (2003), The potential of polarization measurements from space at mm and sub-mm wavelengths for determining cirrus cloud parameters, *Atmos. Chem. Phys.*, *3*, 39–48.

Mishchenko, M. (2000), Calculation of the amplitude matrix for a nonspherical particle in a fixed orientation, *Appl. Opt.*, *39*, 1026–1031.

Mishchenko, M., J. Hovenier, and L. Travis (2000), *Light Scattering by Non-spherical Particles*, Elsevier, New York.

Takano, Y., and K.-N. Liou (1989), Solar radiative transfer in cirrus clouds. Part II: Theory and computation of multiple scattering in an anisotropic medium, *J. Atmos. Sci.*, *46*, 20–46.

Warren, S. (1984), Optical constants of ice from the ultraviolet to the microwave, *Appl. Opt.*, *23*, 1206–1225.

Waters, J., et al. (1999), The UARS and EOS Microwave Limb Sounder (MLS) experiments, *J. Atmos. Sci.*, *56*, 194–218.

Westbrook, C., R. C. Ball, P. Field, and A. Heymsfield (2004), A theory of growth by differential sedimentation, with application to snowflake formation, *Phys. Rev. E*, *70*, 021403, doi:10.1103/PhysRevE.70.021403.

R. E. Cofield, J. H. Jiang, and D. L. Wu, Jet Propulsion Laboratory, California Institute of Technology, Pasadena, CA 91109–8099, USA.

C. P. Davis and R. S. Harwood, Institute of Atmospheric and Environmental Science, University of Edinburgh, Edinburgh EH93JZ, UK. (cdavis@staffmail.ed.ac.uk)

C. Emde, Institute for Envronmental Physics, University of Bremen, D-28359 Bremen, Germany.